Complexation of the Carbonate, Nitrate, and Acetate Anions with the Uranyl Dication: Density Functional Studies with Relativistic Effective Core Potentials†

Wibe A. de Jong,*,‡ Edoardo Aprà,‡ Theresa L. Windus,‡ Jeffrey A. Nichols,§ Robert J. Harrison,§ Keith E. Gutowski,|| and David A. Dixon*,||

Environmental Molecular Sciences Laboratory, Pacific Northwest National Laboratory, P.O. Box 999, Richland, Washington 99352, Oak Ridge National Laboratory, Computer Science and Mathematics Division, PO Box 2008, Oak Ridge Tennessee 37831, and Chemistry Department, University of Alabama, Tuscaloosa, Alabama 35487-0336

Received: July 27, 2005; In Final Form: October 6, 2005

The structures and vibrational frequencies of uranyl carbonates, $[UO_2(CO_3)_n]^{(2-2n)}$ and $[(UO_2)_3(CO_3)_6]^{6-}$ uranyl nitrates, $[UO_2(NO_3)_n]^{(2-n)}$, and uranyl acetates, $[UO_2(CH_3COO)_n]^{(2-n)}$ ($n = 1,2,3$) have been calculated by using local density functional theory (LDFT). Only bidentate ligand coordination modes to the uranyl dication have been modeled. The calculated structures and frequencies are compared to available experimental data, including IR, Raman, X-ray diffraction, and EXAFS solution and crystal structure data. The energetics of ligand binding have been calculated using the B3LYP hybrid functional. In general, the structural and vibrational results at the LDFT level are in good agreement with experimental results and provide realistic pictures of solution phase and solid-state behavior. For the $[UO_2(CO_3)_3]^{6-}$ anion, calculations suggest that complexity in the CO_3^{2-} stretching signature upon complexation is due to the formation of C═O and C−O domains, the latter of which can split by as much as 300 cm^{-1}. Assessment of the binding energies indicate that the $[UO_2(CO_3)_2]^{2-}$ anion is more stable than the $[UO_2(CO_3)_3]^{4-}$ anion due to the accumulation of excess charge, whereas the tri-ligand species are the most stable in the nitrate and acetate anions.

Introduction

The subsurface transport of actinide elements, especially U and Pu, is a key issue for the U.S. Department of Energy (DOE) owing to past disposal practices and the potential for future releases resulting from residual material remaining in the waste tanks at the nuclear weapons production sites following closure. In its hexavalent form, uranium usually exists in the environment as the uranyl dication UO_2^{2+} which can form complexes with a variety of anionic species including carbonate, bicarbonate, acetate, and nitrate. These complexes may be mobile and thus can have an important role in the migration of actinide ions in the subsurface. As an example, actinide carbonate complexes can be quite complicated because several ions can exist in equilibria with each other, with the uncomplexed ion, and with complete and partially hydrolyzed species. This complicates the interpretation of experimental measurements, especially those needed to determine thermodynamic equilibria. Molecular-level studies, combined with experimental observations, can provide a fundamental understanding of the microscopic mechanisms of complexation and speciation, for example, the adsorption to surfaces of minerals and mechanisms responsible for conversions between species. The data obtained at a microscopic level can be used to develop macroscopic adsorption models for predicting migration or transport of uranium. As an example, such models for the aqueous complexation of actinides (Th, U, Np, and Pu) with carbonates are important because (1) carbonate is a ubiquitous ligand in groundwater systems; (2) carbonate can form strong aqueous complexes with actinide species; and (3) these complexes can increase the solubility of compounds that may be present in nuclear waste.

Most of the experimental work has focused on the equilibrium chemistry of actinide complexes in various solutions, using potentiometric or solubility methods combined with a variety of spectroscopic techniques. Spectroscopic techniques including X-ray diffraction (on solids), Raman, IR, UV, and ^{13}C NMR, and more recently, EXAFS and ^{17}O NMR, have been employed to measure geometrical and vibrational data in order to obtain a better understanding of the coordination chemistry of uranyl in solids and solutions.[1,2] The most typical uranyl carbonate (UO_2CO_3) is the mineral rutherfordine with an orthorhombic structure containing linear uranyl species. The tricarbonate $UO_2(CO_3)_3^{4-}$ and dicarbonate $UO_2(CO_3)_2^{2-}$ complexes can also be found, both in the solid state and in solution. In addition, the trimeric $(UO_2)_3(CO_3)_6^{6-}$ species has also been observed in solution. In solution, the presence of the various carbonate complexes is strongly dependent on pH.[1] Amayri et al.[3] have used powder X-ray diffraction (XRD), scanning electron microscopy with energy dispersive spectroscopy, time-resolved laser induced fluorescence spectroscopy (TRLFS), XPS and FT-IR to characterize uranium carbonate andersonite, $Na_2Ca[UO_2(CO_3)_3]\cdot 6H_2O$. This group[4] has also studied a series of alkine uranyl carbonates $M[UO_2(CO_3)_2]\cdot nH_2O$ with M = Mg_2, Ca_2, Sr_2, Ba_2, Na_2Ca, and CaMg using XRD, XPS, and EXAFS as well as TRLFS. Frost et al.[5] have studied the uranyl tricarbonate mineral liebigite $Ca_2[UO_2(CO_3)_3]\cdot 11H_2O$ with Raman spectroscopy at 298 and 77 K.

† Part of the special issue "Jack Simons Festschrift".

* To whom correspondence should be addressed. Wibe.DeJong@pnl.gov; dadixon @bama.ua.edu.

‡ Environmental Molecular Sciences Laboratory, Pacific Northwest National Laboratory.

§ Oak Ridge National Laboratory, Computer Science and Mathematics Division.

|| Chemistry Department, University of Alabama.

10.1021/jp0541462 CCC: $30.25
Published on Web 11/18/2005

TABLE 1: Molecules Studied with Their Symmetries

carbonates	symmetry	acetates	symmetry	nitrates	symmetry
CO_3^{2-}	D_{3h}	$CH_3CO_2^-$	C_s	NO_3^-	D_{3h}
UO_2CO_3	C_{2v}	$UO_2(CH_3CO_2)^{1+}$	C_s	$UO_2NO_3^{1+}$	C_{2v}
$UO_2(CO_3)_2^{2-}$	D_{2h}	$UO_2(CH_3CO_2)_2$	C_{2v}	$UO_2(NO_3)_2$	D_{2h}
$UO_2(CO_3)_3^{4-}$	D_{3h}	$UO_2(CH_3CO_2)_3^{1-}$	C_{3v}	$UO_2(NO_3)_3^{4-}$	D_{3h}
$(UO_2)_3(CO_3)_6^{6-}$	D_{3h}				

For the nitrates, the amount of available spectroscopic data is limited. The structure of crystalline $UO_2(NO_3)_2(H_2O)_2 \cdot 4H_2O$ has been determined by neutron diffraction.[6] Most of the experimental work on the uranyl nitrates has been done using Raman spectroscopy. Brooker et al.[7] studied the spectra of $UO_2(NO_3)_2$ in melts and solution. Nguyen-Trung et al.[8] have measured symmetric stretches of uranyl in solution with various ligands, including nitrate and acetate, and different coordination environments in order to understand the trends of ligand bonding for speciation purposes. De Houwer et al. have reported the UV−vis spectra of the nitrates.[9]

We are interested in using high accuracy computational chemistry approaches to provide insight into fundamental processes involving the actinides. Only within the past few years have calculations appeared that incorporate relativistic effects on compounds that are of real interest to experimentalists and to the DOE cleanup effort. For the carbonate complexes, a variety of calculations have been reported on the $UO_2(CO_3)_3^{4-}$ anion[10−13] and on the UO_2CO_3 molecule.[14−16] However, most of these studies have focused on the geometries and only one report contained any calculated frequencies. For the nitrate complexes, most of the prior calculations have been on the structure of uranyl with two nitrate and two water groups. Ryzhkov et al.[17] reported DV-Xα calculations on the $UO_2(NO_3)_2 \cdot 2H_2O$ crystal. Craw et al.[18] performed geometry optimizations and calculated ligand binding energies of $UO_2(NO_3)_2(H_2O)_2$ using the Hay ECP for U with double-ζ quality basis sets. Hirata et al.[19,20] recently reported DV-DS calculations on this structure to analyze their valence XPS spectra of the crystal. A more extensive study on the bond strength of, and the relative bonding between, ligands was done by Oda et al.[21] using DV-DS to study $UO_2X_2L_2$ structures with X = Cl, NO_3 and L = TBP, TMP, TBPO.

There has been a significant amount of experimental work on the binding of acetates to uranyl.[22] Structural work and a number of other studies have been summarized by Bailey et al.[23] who present XAS results. Other structural studies include EXAFS studies[24,25] of solids and solutions and X-ray diffraction studies.[26−29] A number of studies of the vibrational spectra have also been performed.[8,30] An interesting result of the experimental work is the potential presence of monodentate binding as well as bidentate bonding when H_2O molecules are also bonded to the uranyl.[25] DFT calculations on the compound $UO_2(CH_3CO_2)_3^-$ have also been reported.[12]

In this paper, we report the results of a theoretical/computational study on a series of uranyl cation and anion complexes: $[UO_2X_n]^{2-n}$ for X = nitrate (NO_3^-) and acetate ($CH_3CO_2^-$) and $[UO_2X_n]^{(2-2n)}$ for X = carbonate (CO_3^{2-}) (labeled as monoligand, diligand, and triligand for $n = 1, 2, 3$, respectively). We also provide results on the carbonate trimer $(UO_2)_3(CO_3)_6^{6-}$. Our focus is on the species with bidentate bonding of the ligands. We have chosen to use density functional theory (DFT) with the relativistic effects treated by using relativistic effective core potentials (RECPs) for our computational approach. Traditional molecular orbital methods based on a single reference configuration work well for most first and second row compounds as well as for many compounds composed of heavier main group elements. However, these methods, in general, do not work as well for many transition metal compounds, even for properties such as geometries and frequencies. DFT[31] has been shown to be an extremely good method for predicting the geometries and frequencies and in many cases, the energetics of compounds involving first, second, and third row transition metals.[32−34] In fact, DFT with a local exchange-correlation potential often provides the best geometries and frequencies for transition metal complexes dominated by ionic interactions. In addition, DFT is proving to be a promising theoretical method for predicting the properties of actinide complexes. For example, Hay and co-workers have studied UF_6, NpF_6, and PuF_6 utilizing the same approach proven so successful with transition metal complexes.[35] This work showed that local DFT (LDFT) calculations using RECPs can quite accurately predict the structures and vibrational frequencies of these actinide fluorides. The local approximation, combining the Slater exchange functional[36] with the Vosko, Wilks, and Nusair correlation functional[37] (SVWN), outperformed the hybrid method, which combines local Slater, nonlocal Becke and exact exchange[38] with the Lee, Yang, and Parr correlation functional[39] (B3LYP), for bond lengths when compared to experiment and in general gave better vibrational frequencies than B3LYP. We also have studied the uranyl ion in detail at high levels of theory and have found that LDFT calculations provide excellent agreement with fully relativistic CCSD(T) calculations.[40]

Details of the Calculations

The molecules studied in this paper with their symmetries are given in Table 1, and their optimized structures are shown in Figures 1 (carbonates), 2 (nitrates), and 3 (acetates). Our previous studies[40] on UO_2^{2+} have shown that good agreement as compared to the fully relativistic CCSD(T) calculations can be obtained with the small core Stuttgart RECP and associated Stuttgart orbital basis sets[41] for U and valence triple-ζ plus polarization (TZVP) DFT optimized basis sets for the oxygen atoms.[42] All of our DFT geometry optimizations and frequency calculations were done with the Stuttgart small core RECPs and the corresponding Stuttgart orbital basis sets for the U atom and the TZVP orbital basis set for all nonactinide atoms. In all cases, spherical basis sets were employed. The most diffuse s-, p-, d- and f-functions in the U basis set, those with an exponent of 0.005, were eliminated. These were deleted due to the difficulty in converging the wave function with such diffuse functions, in part due to the types of grids that were used. Additional calculations with the full U basis set, including the diffuse functions, were done only for the $[UO_2(CO_3)_3]^{4-}$ and $[(UO_2)_3(CO_3)_6]^{6-}$ molecules.

The local exchange and correlation functional SVWN described above has been used to determine the structures and frequencies. To assess the dependence of the results on the functional, the structures and frequencies for the uranyl tricarbonate were determined using the PBE96 gradient corrected functional.[43] Binding energies were determined using the B3LYP exchange-correlation functional. We did not use fitting for the Coulombic part of the DFT calculations although we

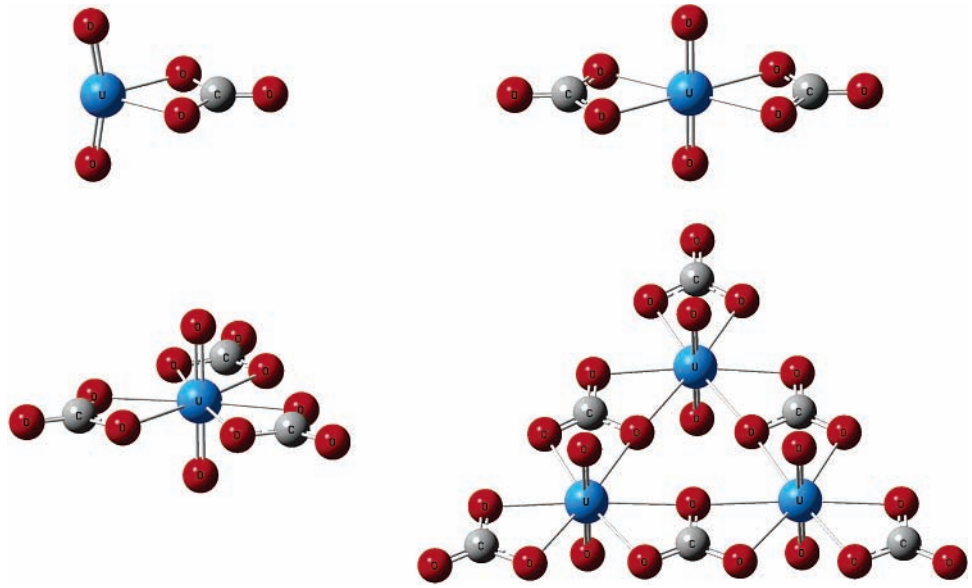

Figure 1. Optimized structures of $UO_2(CO_3)$, $UO_2(CO_3)_2^{2-}$, $UO_2(CO_3)_3^{4-}$, and $(UO_2)_3(CO_3)_6^{6-}$.

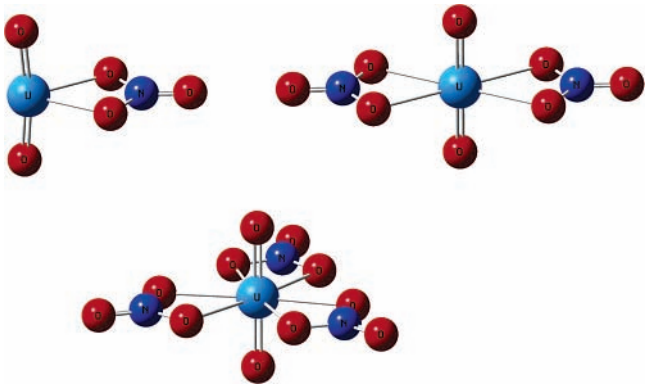

Figure 2. Optimized structures of $UO_2(NO_3)^+$, $UO_2(NO_3)_2$, and $UO_2(NO_3)_3^-$.

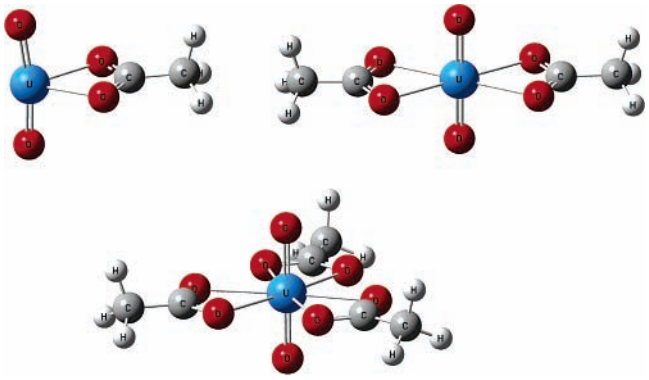

Figure 3. Optimized structures of $UO_2(CH_3COO)^+$, $UO_2(CH_3COO)_2$, and $UO_2(CH_3COO)_3^-$.

advocate the use of the Dunlap fit[44] to reduce the cost of DFT calculations and have started work in our laboratory to determine accurate fitting basis sets for the actinide orbital sets. Because of the diffuse nature of the Stuttgart orbital sets, great care had to be taken in the numerical integration of the density and exchange and correlation functionals. Very large radial and angular grids were employed in order to achieve the desired convergence of 1.0×10^{-8} in the total energy and 1.0×10^{-4} in the geometric gradient. Most of the calculations were done with the program NWChem[45] and a few were done with the program Gaussian03.[46] Natural Bond Orbital (NBO) analyses[47] were performed at the optimized goemetries at the local DFT level with the program Gaussian03.

Results and Discussion

Carbonate Geometries. In Table 2, we compare the bond lengths between theory and experiment for the uranyl tricarbonate anion. The calculated values at the simplest LDA level show reasonable agreement with the experimental results[1,2,4,48−52] with the U═O bond distances 0.03 to 0.05 Å too long. Both the C−O distances and the U−C distances are in good agreement with experiment. The $U-O_{eq}$ distances are ∼0.03 to 0.04 Å too long and the U--O (terminal C═O) bond distance is too long by ∼0.05 Å. The inclusion of the diffuse U basis functions, see details of the calculations section, improves the agreement with experiment. The U═O distance shortens and the carbonate groups get closer to the experimental values. The calculations on the isolated uranyl tricarbonate anion in the gas phase confirm the experimental determinations of the structure of the complex in the solid and in solution. Using the PBE96 gradient corrected functional makes the agreement with experiment worse. This is consistent with other DFT calculations on metals which show that gradient corrected functionals tend to predict bond distances that are too long in transition metal complexes. We note that calculations at the PW91/ZORA/TZP/DZP level give bond distances that are systematically too long.[12] In addition, MBPT2 calculations with a large basis set and ECPs give a structure in the gas phase with bond distances that are far too long.[11] To improve agreement with experiment, the MBPT2 calculations were also done using an SCRF approach with a spherical cavity. The U═O distance is still too long and the CO_3^{2-} fragment becomes strongly distorted but the bonding of the carbonate with the UO_2^{2+} is improved. The use of the COSMO model at the PW91 level also led to improved structures.[12] Tsushima et al.[13] have predicted the structure of the tricarbonate at the DFT level with the B3LYP functional and a variety of basis sets with large core ECPs. Their uranyl U═O bond distances show similar values to ours but their $U-O_{eq}$ distances are up to 0.1 Å longer as compared to our values and to experiment.

The bond distances for the trimer $(UO_2)_3(CO_3)_6^{6-}$ are shown in Table 3. Addition of the diffuse functions to the U at the LDA level leads to decreases in the U═O bond length as well

TABLE 2: Comparison of Calculated and Experimental Bond Distances (Å) for $UO_2(CO_3)_3^{4-}$

method	U═O	C═O	C−O	U−O	U−C	U- -O
LDA	1.835	1.280	1.304	2.462	2.916	4.197
LDA + diffuse	1.815	1.264	1.300	2.430	2.902	4.166
PBE96	1.825	1.277	1.311	2.527	2.994	4.271
MBPT2	1.894	1.297	1.321	2.426	2.893	4.790
PW91/ZORA[12]	1.85			2.56	3.01	4.29
EXAFS/soln[2]	1.80 ± 0.02			2.43 ± 0.02	2.89 ± 0.04	4.13 ± 0.04
X-ray/solid[a,1]	1.79			2.42	2.89	4.12
EXAFS/solid[a,1]	1.80	mean: 1.288		2.43	2.89	4.13
X-ray/solid[48]	1.77−1.78			2.434		
X-ray/solid[b,49]	1.78−1.81	1.29	1.26−1.31	2.41−2.46		
X-ray/solid[c,50]		1.25 ± 0.01	1.29 ± 0.01	2.43 ± 0.03		
EXAFS/solid[d,52]	1.80−1.81			2.42−2.44	2.89−2.90	4.10−4.22
X-ray/solid[e,51]	1.802	1.24	1.31	2.43	2.87−2.88	4.09−4.12
EXAFS/solid[f,4]	1.80			2.45	2.90	4.20
EXAFS/solid[g,4]	1.80			2.43	2.88	4.15
EXAFS/solid[h,4]	1.81			2.43	2.90	4.16
EXAFS/solid[i,4]	1.81			2.44	2.89	4.19
EXAFS/solid[j,4]	1.79			2.43	2.88	4.15
EXAFS/solid[k,4]	1.79			2.44	2.90	4.21

[a] $K_4[UO_2(CO_3)_3]_4$. [b] $Na_2CaUO_2(CO_3)_3$. [c] $Ca_2[UO_2(CO_3)_3]$. [d] $UO_2(CO_3)_3^{4-}$. [e] $K_4UO_2(CO_3)_3$. [f] $Mg_2UO_2(CO_3)_3$. [g] $Ca_2UO_2(CO_3)_3$. [h] $Sr_2UO_2(CO_3)_3$. [i] $Ba_2UO_2(CO_3)_3$. [j] $Na_2CaUO_2(CO_3)_3$. [k] $CaMgUO_2(CO_3)_3$.

TABLE 3: Comparison of Calculated and Experimental Bond Distances (Å) for $(UO_2)_3(CO_3)_6^{6-}$

method	U═O	C═O	C−O	U−O	U−C	U- -O	U- -U
LDA	1.811	1.303[a]	1.307[b]	2.422[b]	2.916[e]	4.155	5.104
		1.275[c]	1.282[d]	2.449[d]	2.880[f]		
				2.554[a]			
				2.475 avg	2.904 avg		
LDA + diffuse	1.796	1.310[a]	1.289[b]	2.489[b]	2.852[e]	4.125	4.937
		1.267[c]	1.275[d]	2.403[d]	2.936[f]		
				2.471[a]			
				2.454 avg	2.894 avg		
X-ray/solid[1]	1.78	1.33[a]	1.26[d]	2.411[b]	2.88	4.14	4.97
		1.27[c]		2.458[d]			
				2.492[a]			
				2.454 avg			
EXAFS/solid[1]	1.79			2.45	2.90	4.16	4.91
EXAFS/soln[1]	1.79			2.46	2.90	4.17	4.92
X-ray/soln[53]	1.80			2.43			4.94

[a] Bridging O-bridging C. [b] Inner O-terminal C. [c] Terminal O-terminal C. [d] Outer O-bridging C. [e] Bridging C. [f] Terminal C.

as the C−O bond lengths. The U−O bond distance to the inner O-terminal C increases by ∼0.07 Å and the U−O bond distance to the bridging O-bridging C decreases by a comparable value. The U−C bond to the bridging C becomes shorter with the additional functions as compared to the U−C bond to the terminal C, the opposite of what is predicted without them. The U- -U non bonding interaction distance decreases by 0.17 Å. Thus, addition of the diffuse functions makes the structure more compact as the carbonates bind more strongly to the uranyl dications. Both calculations give good agreement with the experimental results.[1,53] The predicted U═O bond distances are within 0.02 to 0.03 Å of the experimental values and are a little too long consistent with the fact that the calculations are for an isolated ion with a charge of −6 whereas the experimental results include the effects of counterions and/or solvent. The C−O distances are consistent with the experimental observations. The average U−O bond distances are in excellent agreement with the experimental values. The LDA values without the additional diffuse functions agree with the X-ray values slightly better as the same ordering is found. However, the calculations with the diffuse functions give a better prediction of the U- -U interaction.

The above results show that we are able to make reliable predictions of the geometries of these highly charged carbonates at the LDA level. In Table 4, we present the variation in the various bond distances for the different types of carbonates that were studied. The addition of a carbonate to UO_2^{2+} increases the U═O bond distance by 0.075 Å and leads to a substantial distortion in the carbonate such that the terminal C═O distance is much shorter than the C−O bond distances of the O atoms bonded to the U. The OUO bond angle deviates from the linearity found in the isolated dication and is 163.8°. This deviation from linearity is a general feature of structures which do not require a linear UO_2^{2+} moiety by symmetry and is indicative of the low bending frequency of the UO_2^{2+} group. Our results differ somewhat from the results of Majumdar et al.[14,15] who used a different ECP and basis set. They found a distance of 1.687 Å for the U═O distance in UO_2^{2+} at the B3LYP level and a U═O distance of 1.756 Å and 1.749 Å (larger basis) for UO_2CO_3 at the same level. At the MP2 level,

TABLE 4: Bond Distances (Å) for the Uranyl Carbonates $UO_2[CO_3]_n^{(2n-2)-}$ $n = 0-3$ and for the Trimer $(UO_2)_3(CO_3)_6^{6-}$

n	total charge (uranyl NBO group charge)	U═O	C═O	C−O	U−O	U−C	U- -O
0	+2 (+2.00)	1.703					
1	0 (+1.09)	1.776	1.199	1.355	2.136	2.652	
2	−2 (+0.76)	1.814	1.239	1.326	2.295	2.755	
3	−4 (+0.64)	1.835	1.280	1.304	2.462	2.916	4.197
trimer averages	−6 (+0.79)	1.811	1.289	1.294	2.475	2.904	4.155

TABLE 5: Comparison of Calculated and Experimental Vibrational Frequencies (cm^{-1}) for $UO_2(CO_3)_3^{4-}$

	U═O (asym)	U═O (sym)	C═O stretch sym ν_1	C═O stretch asym ν_3	C−O stretches	CO_3^{2-} out of plane ν_2	CO_3^{2-} in plane $\nu 4$
LDA	827	760	1533 a_1'	1508e′	1039e′ 1045a_1' 1356a_2' 1383e′	845a2" 834e"	692e′ 642e′ 634a_2'
LDA + diffuse	872	783	1491	1469e	1041e	814	598e 612e
PBE96	862	778	1438	1420e	1008e	806	590e 603e
Raman/soln[8]		812 ± 3					
Raman/soln[1]		812.5					
Raman/solid[a,1]	889					894	
Raman, IR/solid[b,57]	882 ir	806 R	1569 R	1600 ir	1358 ir, 1354 R, 1045 ir, 1046 R	855 ir, 879 R	694 719 ir
Raman/soln[56]		812	1545		1378, 1064.5		681 735
Raman/soln[55]		815		1460	1295, 1065, 1002		
Raman, IR/solid[c,58]	843 ir	808 R	1630 R	1560 ir	1342 ir, 1358 R 1062 ir, 1077 R	821 ir	700, 732 ir
Raman/solid[d,52]		818 ± 2					
FTIR/solid[e,3]	902			1571,1526	1383, 1092, 1080		727, 700

[a] IR estimated. [b] $K_4[UO_2(CO_3)_3]$. [c] $Na_4[UO_2(CO_3)_3]$. [d] Uranyl-doped calcite. [e] Synthetic $Na_2Ca[UO_2(CO_3)_3]\cdot 6H_2O$.

TABLE 6: Comparison of Calculated and Experimental Vibrational Frequencies (cm^{-1}) for $(UO_2)_3(CO_3)_6^{6-}$

method	U═O (asym)	U═O (sym)	C═O stretch sym ν_1	C═O stretch asym ν_3	C−O stretches	CO_3^{2-} out of plane ν_2	CO_3^{2-} in plane $\nu 4$
LDA	880e 892	801, 794e	1546 1444	1531e 1428e	1357e, 1356, 1065, 1058e, 1042e, 1041		
LDA + diffuse	909e 922	832e		1476e 1573e	1399e 1413e 1059e 1064e	806 810	565e 595e 686e 707e
Raman/soln[8]		834					
Raman/soln[1]		831.6					

TABLE 7: Trends in Selected Calculated Vibrational Frequencies (cm^{-1}) for the Uranyl Carbonates $(UO_2[CO_3]_n)^{(2n-2)-}$ and $(UO_2)_3(CO_3)_6^{6-}$

N	charge	U═O (asym)	U═O (sym)	C═O	C−O	CO_3 inversion
CO_3^{2-}				1389(asym),	1008(sym)	852
0	+2	1123	1019			
1	0	951	880	1819	1033, 956	757
2	−2	883	805	1663, 1648	1237,1225 1014, 1012	807,806
3	−4	827	760	1533, 1508(e)	1356a_2' 1383e′ 1039e′ 1045a_1'	845a_2'', 834e″
trimer	−6	880e, 892	801, 794e	1444, 1428(e) 1546, 1531(e)		

their best calculation gave 1.728 Å for UO_2^{2+} and 1.784 Å for UO_2CO_3. At the CASSCF level, the U═O bond distance of 1.697 Å in UO_2CO_3 is clearly too short. Addition of a second carbonate leads to an increase of 0.038 Å in the U═O bond distance and the uranyl becomes linear again in the higher symmetry that is available. The distortion in the carbonate also decreases and the U−O distances substantially increase. The addition of the final carbonate leads to an increase in the U═O bond distance of 0.021 Å and the carbonate C−O distances become almost equal and close to the calculated C−O bond distance for CO_3^{2-} of 1.309 Å. The U−O distances lengthen out to the values observed in the experimental measurements as discussed above. The U−O distances are also in agreement with the original X-ray study on solid-state UO_2CO_3, rutherfordine by Cromer et al.,[54] who found U−O distances of 2.52 and 2.42 Å. They also found that UO_2 is linear with a U═O bond distance of 1.67 ± 0.09 Å. We favor the higher range of the bond distance. The uranyl trimer exhibits interesting values when compared to the other carbonates. The U═O bond distance is essentially the same as the value for $UO_2(CO_3)_2^{2-}$ consistent with the charge on the system yet the carbonate groups more closely resemble the geometry in $UO_2(CO_3)_3^{4-}$.

The NBO group charges for the UO_2^{2+} (charge on the U plus the two axial O atoms) in the carbonates are given in Table 4. The NBO group charges show that there is ∼0.9 e transferred to the uranyl in the monocarbonate to reduce the positive charge on the uranyl. In the dicarbonate, ∼1.25 e is transferred to the uranyl and ∼1.35 e in the tricarbonate. In the trimer, the amount of charge transferred to the uranyl is ∼1.20 e, slightly less than found for the dicarbonate. These amounts of charge transfer are consistent with the geometry changes and with the changes in the uranyl vibrational frequencies.

Carbonate Frequencies. Selected calculated frequencies for the tricarbonate are given in Table 5 where they are compared to the available experimental data and for the trimer in Table 6. The uranyl and CO stretching frequencies for all of the carbonates are given in Table 7. The complete listings of the frequencies with their assignments are given as Supporting Information. We focus on the uranyl stretches and the carbonate C−O stretches in our discussion. The UO_2 symmetric U═O stretch for the tricarbonate is calculated to be at 760 cm^{-1} at the LDA level. Addition of diffuse functions on the U increases this value to 783 cm^{-1}. The experimental value[1] in solution at pH = 8 is 812.5 cm^{-1} and has been reported to be between 810 and 820 cm^{-1} in solution and in the solid from a variety of experiments.[52,55,56] The LDA value for the asymmetric stretch is calculated to be at 827 cm^{-1} and increases to 872 cm^{-1} with the addition of U diffuse functions. The experimental value for

the asymmetric stretch is difficult to measure in the solid as the carbonate out-of-plane deformation frequencies mask it so it has been estimated to be at 889 cm^{-1}. Other studies reported values of 902 cm^{-1},[3] 893 cm^{-1},[57] and 843 cm^{-1}.[58] Thus there is some variation in the experimental values for this quantity. The LDA values underestimate the experimental values by ~50 cm^{-1}.

The symmetric combination of the carbonate C═O stretches is predicted to be at 1533 cm^{-1} at the LDA level and the asymmetric combination at 1508 cm^{-1}. Addition of diffuse functions to the U lowers the C−O stretches but improving the grid raises them. Use of a gradient corrected potential substantially lowers these frequencies. The C═O stretches in the crystal have been measured from 1545 to 1630 cm^{-1} for the symmetric combination. The calculations predict that the C═O stretches should only split by 20 to 30 cm^{-1}. There is a substantial split between the C═O terminal stretches and the other C−O stretches which are in the range of 1400 and 1000 cm^{-1}. The lower range of predicted values near 1040 to 1050 cm^{-1} is in good agreement with the experimental values near 1050 to 1060 cm^{-1}.[52,55,57,58] The higher range of calculated values near 1350 to 1390 cm^{-1} are in good agreement with the experimental values reported between 1340 and 1380 cm^{-1}.[55,57,58] The stretching bands for CO_3^{2-} are predicted to be at 1389 and 1008 cm^{-1}. Thus, the calculations show that the splitting of the carbonate bands on complexation is really due to formation of the C═O species and that the remaining bands actually have similar splittings to that in the free ion. It has been suggested that in general the ν_3 carbonate ligand stretch (asymmetric) is split into two components upon coordination to metal ion, 50−60 cm^{-1} for monodentate and 160−190 cm^{-1} for bidentate.[1] This is consistent with our results but the splitting is due to formation of the C═O bonds. We also find that there is an even larger splitting of the ν_1 symmetric carbonate stretch by almost 500 cm^{-1} due to formation of the C═O terminal bonds. The out of plane bends for the carbonate are predicted to be 20 to 50 cm^{-1} below those measured in the solid for most cases[1,57,58] and the in-plane bends are predicted to be a similar amount below the experimental values.[52,57,58] Whether this is due to differences in the solid state and the isolated ion or to the computational methods is difficult to determine but the overall good agreement with experiment shows that the computational approach is providing a reliable prediction of the geometry and vibrational frequencies.

For the trimer, there are six UO_2 stretching modes. The symmetric coupling of the symmetric stretch is predicted to be at 801 cm^{-1} and the degenerate asymmetric coupling at 794 cm^{-1}. The symmetric coupling of the asymmetric stretches is predicted to be at 892 cm^{-1} and the degenerate asymmetric coupling of the asymmetric stretches is predicted to be at 880 cm^{-1}. Adding diffuse functions to the U raises the stretches by ~30 cm^{-1}, less than predicted for the tricarbonate which has a higher negative charge at the uranyl. The experimental values are 831.6 cm^{-1} at pH = 6 and 834 cm^{-1}.[1,8] Thus, the calculated values are within 30 cm^{-1} of the experimental ones. The UO_2 asymmetric stretch has been estimated[1] from experiment to be 911 cm^{-1} in good agreement with our values. The C−O stretches split into a number of groups. The terminal C═O stretches in the terminal CO_3 groups are predicted to be near 1540 cm^{-1}. The highest energy stretches in the bridging carbonyls are predicted to be about 100 cm^{-1} lower. The remaining C−O stretches split into two groups as found in the tricarbonate with one group near 1350 cm^{-1} and the larger group near 1050 cm^{-1}.

Selected calculated frequencies for the various carbonates are compared to each other in Table 7. The U═O symmetric and asymmetric stretches decrease with increasing the number of carbonates added to the UO_2^{2+}. This is consistent with donating negative charge into the UO_2^{2+} thereby decreasing the interaction of the positively charged uranium with the negatively charged axial oxygens (see NBO charges in Table 4). It is clear from the calculations that the uranyls in the trimer are closest to the uranyl in the dicarbonate dianion as the frequencies in both are comparable even though the environment about the uranyls are somewhat different in the two species. There is also a significant trend in the C═O terminal stretches. In the mono carbonate, the C═O stretch is like that in a carbonyl with a frequency above 1800 cm^{-1}. The C−O frequencies are like that of the symmetric stretch in the isolated dianion. There is a decrease of about 150 cm^{-1} in the terminal C═O stretch when the second carbonate is added consistent with an increase in this bond distance as the carbonate becomes less distorted. The C−O stretches split significantly with one pair near 1230 cm^{-1} and one pair near 100 cm^{-1}, with the latter pair being near the symmetric stretch in the isolated carbonate dianion. The C═O stretches decrease by another 130 to 140 cm^{-1} when the third carbonate is added. The C−O stretches, as discussed above, are substantially split and resemble those in the isolated dianion. Even though the uranyls in the trimer are like that in the dicarbonate, the terminal carbonates are like that in the tricarbonate in terms of the terminal C═O stretch. The highest energy stretches in the bridging carbonates are predicted to be almost 100 cm^{-1} below the C═O terminal stretches in the trimer and are unlike any of the other carbonates. The other C−O stretches are like those in the tricarbonate. There is a substantial decrease in the out of plane inversion mode at C going from the isolated carbonate dianion to the monocarbonate consistent with loss of the resonance averaging about the carbon with the unequal C−O bonds. This inversion frequency increases as the carbonate groups more closely resemble the parent so that in the tricarbonate, the inversion frequencies are quite similar to those in the isolated carbonate.

Majumdar et al.[14,15] have reported U−O stretching frequencies for $UO_2(CO_3)$ with one, two and three waters at the MP2 and B3LYP levels. The results at the MP2 level are 846, 841, 841, and 835 cm^{-1} for the symmetric stretch for zero, one, two and three waters respectively, and 920, 925, and 916 cm^{-1} for the asymmetric stretch for one, two, and three waters, respectively. At the B3LYP level, they reported 882, 870, and 862 cm^{-1} for the symmetric stretch for zero, two, and three waters respectively and 954 and 947 cm^{-1} for the asymmetric stretch for two and three waters, respectively. These results are consistent with our calculated values of 880 and 951 cm^{-1} for the symmetric and asymmetric stretches, respectively.

Nitrate Structures. The key geometry parameters in the nitrates are given in Table 8. The geometries show the trends found in the carbonate calculations. As more negative charge is placed about the uranyl, the U═O bond distance increases (see NBO charges in Table 8). Because the charge on the complexing anion is only one for the nitrates, the change per ligand added is smaller than in the carbonates. The mononitrate uranyl group charge is +1.41 e as compared to the monocarbonate group charge of +1.09 e. The U═O bond distance in the neutral dinitrate is 0.01 Å shorter than the U═O bond in the neutral monocarbonate and the trinitrate with one negative charge has a U═O bond which is 0.01 Å longer than the neutral monocarbonate. The UO_2^{2+} moiety is more nearly linear in the mononitrate, $<OUO = 171.4°$, as compared to the carbonate

TABLE 8: Calculated and Experimental Geometrical Parameters (Bond Distances in Å) of the Uranyl Nitrates ($[UO_2]^{2+}[NO_3]_n^{n-}$)

N	total charge (uranyl NBO group charge)/ compound	U═O	N−O_t	N−O	U−O	U−N
0	+2 (+2.00)	1.703				
1	+1 (+1.41)	1.742	1.177	1.309	2.258	2.746
2	0 (+1.09)	1.766	1.198	1.291	2.361	2.813
3	−1 (+0.84)	1.784	1.215	1.281	2.426	2.867
X-ray/solid[62]	$0/UO_2(NO_3)_2(H_2O)_3$	1.742			2.497	
X-ray/solid[61]	$-1/KUO_2(NO_3)_3$	1.755	1.201	1.273	2.482	
Neutron/solid[59]	$-1/RbUO_2(NO_3)_3$	1.78	1.22	1.25	2.48	
Neutron/solid[60]	$-1/CsUO_2(NO_3)_3$	1.77			2.52	
IR/solid[a,63]	$0/UO_2(NO_3)_2 \cdot 6H_2O$	1.715				
IR/solid[a,63]	$0/UO_2(NO_3)_2 \cdot 3H_2O$	1.710				
IR/solid[a,63]	$-1/KUO_2(NO_3)_3$	1.705				
IR/solid[a,63]	$-1/CsUO_2(NO_3)_3$	1.700				
IR/solid[a,63]	$-1/NH_4UO_2(NO_3)_3$	1.700				

[a] Obtained by a correlation of the force constants.

as more charge is transferred from the carbonate as compared to the nitrate. Experimental data from X-ray crystal structures of the nitrates are consistent with the calculated values. The U═O bond lengths in the Rb and Cs salts of $UO_2(NO_3)_3^-$ are in excellent agreement with the predicted values for the monoanion, but the same bond length in the K salt is 0.03 Å is shorter.[59−61] The experimental U−O_{eq} bond lengths in the K, Rb, and Cs salts of the monoanion are 0.06, 0.05, and 0.09 Å longer than the predicted values, respectively, while the N−O bond lengths agree with experiment to within 0.01−0.03 Å. The U═O bond length in the crystal structure of $UO_2(NO_3)_2(H_2O)_3$ is 0.024 Å shorter than that predicted for the neutral $UO_2(NO_3)_2$ species.[62] In addition, the predicted U−O_{eq} bond lengths are 0.14 Å shorter than in the $UO_2(NO_3)_2(H_2O)_3$ crystal structure. This is consistent with the fact that the water molecules are forcing the nitrate away from the uranyl leading to the increased U−O_{eq} bond length. Because the nitrates are interacting less strongly with the uranyl, the U═O bond distances will be shorter. The presence of water molecules is expected to lengthen the U═O bond distance but the fact that they are neutral means that the effect is smaller than the interactions with an anion. Additional solid state structural data were obtained from a correlation of the uranyl force constants obtained from infrared measurements. The calculated and crystal structure values clearly show a different trend from the infrared data[63] which show little variation with the charge for the U═O bond distance and in fact show the trinitrate anion with a bond distance shorter than the neutral dinitrate and comparable to that predicted for the isolated UO_2^{2+} ion. This suggests that the correlation of bond distance with stretching frequencies is not properly describing the geometry of the nitrate complexes.

The NBO group charges on the nitrates show an interesting trend (Table 8). For the mononitrate, ∼0.60 e is transferred to the uranyl, substantially less than the transfer of ∼0.90 e for the monocarbonate. For the dinitrate, the charge transfer of ∼0.90 e to the uranyl is the same as that for the monocarbonate consistent with an overall neutral species. For the trinitrate, the charge transfer of ∼1.15 e to the uranyl is less than that transfer of ∼1.25 e found in the dicarbonate, consistent with the fact that the trinitrate complex has a −1 charge and the dicarbonate has a −2 charge.

Nitrate Frequencies. Selected calculated nitrate frequencies are given in Table 9 and are compared to the available experimental values. As would be expected from the carbonate study and the nitrate geometries, the uranyl frequencies decrease with increasing numbers of ligands but the range is smaller. The frequencies for the neutral dinitrate and the anionic trinitrate bracket the U═O stretches for the neutral monocarbonate. The calculated frequencies are consistent with the experimental stretching frequencies for the nitrates that have been reported.[63,64] Again, the experimental values for the trinitrate anion are larger than those for the neutral dinitrate which is not consistent with our results or with simple chemical models. This suggests that there may be complicating factors in the experimental measurements. For example, water molecules are likely to be complexed to the uranyl which would lower the U═O stretching frequencies and potentially make the uranyl stretch in the neutral diacetate less than that in the anionic triacetate.

The NO stretches have the same behavior as observed for the carbonates. The NO stretches are split by almost 350 cm^{-1} in the isolated anion with the asymmetric stretch at 1400 cm^{-1} and the symmetric stretch at 1060 cm^{-1}. Complexation to the uranyl dication splits the stretches so that there is a high-frequency mode for the terminal N−O near 1740 cm^{-1} and two lower frequency modes which bracket the symmetric stretch in the nitrate anion by about 50 to 60 cm^{-1}. Complexation of the second nitrate lowers the terminal stretches by 70 to 90 cm^{-1} and increases the splitting of the other N−O modes. The lower energy modes are now comparable to those in the isolated anion. Complexation of the third anion lowers the terminal stretches again and increases the splitting in the other N−O modes. However, the higher frequency N−O modes involving complexation to the uranyl are still not as high as the asymmetric stretch in the isolated anion by almost 100 cm^{-1} in contrast to what is observed in the carbonate series.

Acetate Structures. The acetate geometries are shown in Table 10. Compared to the nitrate, the uranyl bond distances are longer than those for the comparably charged species. This is consistent with the acetate having its negative charge more strongly localized in the CO_2 fragment in contrast to having some of the charge localized on the terminal oxygen as found for the nitrate. As a consequence, the uranyl moiety sees more negative charge and the U═O bond distances are longer. The NBO uranyl group charge for the monoacetate is +1.35 e as compared to the group charge of + 1.41 e on the mononitrate, consistent with this simple model. The calculated structure for the triacetate is in good agreement with the experimental structures within a few hundredths of an Å for all geometry parameters.[24−29] The U═O bond distance is predicted to be too long by 0.02 Å as expected based on the results for the other anions. We note that a proper treatment of the thermal corrections in the X-ray structures as reported[26] gives better agreement with our calculated structure. The EXAFS data[20,21] predict similar geometry parameters and the values are similar to our values as well as to those determined by X-ray diffraction. The EXAFS solution result agrees extremely well with the calculated diacetate structure. Calculations at the PW91/DZVP/TZVP level with ADF[12] give a U═O bond distance of 1.81 Å with or without solvent corrections and U−O_{eq} distances of 2.51 Å in contrast to our values of 1.79 and 2.44 Å which are in better agreement with experiment. Again, the monoacetate does not have a linear UO_2^{2+} moiety with ∠OUO = 169.8°.

The NBO group charges on the acetates (Table 10) behave similarly to those for the nitrates. For the monoacetate, ∼0.65 e is transferred to the uranyl, for the diacetate, ∼0.95 e is transferred to the uranyl, and ∼1.15 e is transferred to the uranyl for the triacetate. The U═O bond distances in the mono- and dinitrate are shorter than the U═O bond distances in the diacetate. This is consistent with the uranyl NBO charges which

TABLE 9: Selected Calculated and Experimental Vibrational Frequencies (cm^{-1}) of the Uranyl Nitrates ($[UO_2]^{2+}[NO_3]_n^{n-}$)

N	charge/ compound	U═O (asym)	U═O (sym)	N−O_t	N−O
NO_3^-	−1			1400(e′)	1060 (a_1′)
0	+2	1123	1019		
1	+1	1038	947	1736 (a_1)	1108 (b_1), 998 (a_1)
2	0	994	906	1665 (a_g), 1651(b_{3u})	1123 (b_{2u}), 1216 (b_{1g}) 1036 (a_g), 1034 (b_{3u})
3	−1	948	860	1605 a_1′, 1582(e)	1298 (e′), 1278 (a_2′) 1054 (a_1′), 1051 (e′)
Raman/soln[8]	+1		870		
Raman,IR/solid[63]	0/$UO_2(NO_3)_2$·$6H_2O$	941	863.9		
Raman,IR/solid[63]	0/$UO_2(NO_3)_2$·$3H_2O$	948.1	874		
Raman,IR/solid[63]	−1/$KUO_2(NO_3)_3$	943.1	875.5		
Raman,IR/solid[63]	−1/$CsUO_2(NO_3)_3$	956.2	884.0		
Raman,IR/solid[63]	−1/$NH_4UO_2(NO_3)_3$	967.2	885.7		
Raman/soln[7]	0/$UO_2(NO_3)_2$		871		
Raman/melt[7]	0/$UO_2(NO_3)_2$·$6H_2O$		872	1613, 1547	

TABLE 10: Calculated and Experimental Geometrical Parameters (Bond Distances in Å) of the Uranyl Acetates ($[UO_2]^{2+}[CH_3CO_2]_n^{n-}$)

n	total charge (uranyl NBO group charge)	U═O	C−C	C−O	U−O	U−C
0	+2 (+2.00)	1.703				
1	+1 (+1.35)	1.749	1.453	1.292	2.213	2.630
2	0 (+1.05)	1.775	1.477	1.278	2.334	2.710
3	−1 (+0.85)	1.791	1.496	1.267	2.441	2.809
X-ray/solid[a,26]	−1	1.759,1.756 (1.774, 1.769)	1.498 (1.530)	1.264,1.256 (1.268,1.258)	2.467,2.462 (2.475,2.469)[d]	
neutron/solid[a,27]	−1	1.761	1.491	1.256	2.476	
X-ray/solid[b,29]	−1	1.748	1.510	1.269	2.474	
X-ray/solid[c,28]	−1	1.750		1.251	2.473	
EXAFS/solid[a,24]	−1	1.78			2.48	2.9
EXAFS/solid[a,25]	−1	1.78			2.48	2.88

[a] $Na[UO_2(CH_3COO)_3]$. [b] $[Ni(H2O)6][UO_2(CH_3COO)_3]_2$. [c] $(C_6H_{15}N_4O_2)[UO_2(CH_3COO)_3]$·$(C_2H_4O_2)$·$H_2O$. [d] Numbers in parentheses indicate correction for thermal motion according to riding model.

show less charge transferred from the anionic ligands to the uranyl in the nitrates as compared to the acetates. This behavior is somewhat more complicated in the trimers. As shown in Tables 8 and 10, the amount of charge transferred to the uranyl in the triacetate and in the trinitrate are essentially the same. Thus the U═O bond distance in the acetate trimer should be comparable or shorter to that in the nitrate trimer, yet the opposite is predicted with the U═O bond distance in the triacetate longer than that in the trinitrate. The increase in the uranyl bond length in the triacetate as compared to the trinitrate could be explained by equatorial steric crowding in $UO_2(CH_3COO)_3^-$. The bite angle in the naked ligand is 120.0° in the nitrate and 129.1° in the acetate. Binding one nitrate to the uranyl reduces the bite angle to 109.4° as compared to 114.2° in the monoacetate. In the dinitrate, the bite angle is 113.0° and in the diacetate, it is 118.7°. The bite angle for trinitrate is 114.5° and in the triacetate, the bite angle is 120.4°. Thus, initial binding of the anionic ligand to the uranyl closes down the bite angle, and this angle increases with additional ligands to become more like that in the naked ligand. The increase in the bite angle in the acetate leads to more steric crowding in the triacetate as compared to the trinitrate, and as a consequence, the U═O bond distance increases more in the triacetate than in the trinitrate. In addition, the U−O equatorial bonds are longer in the triacetate than in the trinitrate which is opposite to the trends observed for the mono- and di-ligand species.

Acetate Frequencies. The uranyl stretching frequencies for the acetates are shown in Table 11. The frequencies for the uranyl decrease as expected with the addition of each acetate ligand. The frequencies for the uranyl are lower than those in the nitrates for a comparably charged complex consistent with the differences found in the bond distances and consistent with more charge transfer from the acetate than the nitrate, except as noted above for the triacetate. A variety of experimental

TABLE 11: Selected Calculated and Experimental Vibrational Frequencies (cm^{-1}) of the Uranyl Acetates ($[UO_2]^{2+}[CH_3CO_2]_n^{n-}$)

method	*n*	charge	U═O (asym)	U═O (sym)	CO_2
LDA	0	+2	1123	1019	
LDA	1	+1	1025	940, 931	1508,[a]1418
LDA	2	0	973	888	1516,1507 1497,[a]1488[a]
LDA	3	−1	934	850	1604e,1580 1480,[a]1470e[a]
IR, Raman/soln[30]	0	+2	962	870	
IR, Raman/soln[30]	1	+1	954	861	
IR, Raman/soln[30]	2	0	928	841	
IR, Raman/soln[30]	3	−1		823	
IR/solid[b,63]	3	−1	920	842.2	
IR/solid[c,63]	3	−1	924	852.1	
IR/solid[d,63]	3	−1	927.8	855.1	
IR/solid[d,65]	3	−1	931	856	
IR/soln[66]	3	−1	922		
IR/soln[67]	3	−1	925		
Raman/soln[8]	0	+2		870	
Raman/soln[8]	1	+1		861	
Raman/soln[8]	2	0		852	
Raman/soln[8]	3	−1		843	

[a] significant mixing with C−C stretch. [b] $CsUO_2[CH_3CO_2]_3$. [c] $RbUO_2[CH_3CO_2]_3$. [d] $NaUO_2[CH_3CO_2]_3$.

TABLE 12: B3LYP Absolute and Relative Binding Energies in kcal/mol for the Uranyl−Anion Complexes ($UO_2[CO_3]_n^{(2n-2)-}$), ($UO_2[NO_3]_n^{(n-2)-}$), and ($UO_2[CH_3CO_2]_n^{(n-2)-}$)

n	CO_3^{2-} absolute[a]	CO_3^{2-} relative to (*n*-1)[b]	NO_3^- absolute[a]	NO_3^- relative to (*n*-1)[b]	$CH_3CO_2^-$ absolute[a]	$CH_3CO_2^-$ relative to (*n*-1)[b]
1	−628	628	−324	324	−364	364
2	−811	183	−505	181	−554	190
3	−645	−167	−581	76	−613	59

[a] $[UO_2]^{2+} + n[\text{Anion}]^{m-} \rightarrow UO_2[A]_n^{(nm-2)-}$. [b] $UO_2[A]_n^{(nm-2)-} \rightarrow UO_2[A]_{n-1}^{((n-1)m-2)-} + [A]^{m-}$.

measurements[8,30,65−67] give U═O stretching frequencies smaller than our calculated values in contrast to what is found for the carbonates. Our isolated monoacetate frequencies are higher than the experimental values by ∼70 cm^{-1} suggesting that there are a number of water molecules complexed to the uranyl which lower the U═O stretching frequencies. The agreement with experiment improves as more acetates are added presumably displacing waters of hydration in aqueous solution.

The C−O modes show interesting behavior. The highest frequency C−O modes increase as more acetates are added. We note that there is a strong coupling of the symmetric stretch of the CO_2 with the C−C stretch leading to a significant splitting of these frequencies in the diacetate.

Binding Energies. We have previously shown for the Ca^{2+} and Sr^{2+} carbonates (and hydroxides) that the DFT binding energies defined as

$$M[CO_3]_n^{(2n-2)-} \rightarrow M[CO_3]_{n-1}^{(2n-4)-} + [CO_3]^{2-}$$

can be related linearly to solution phase equilibrium constants.[68] The calculated binding energies at the B3LYP level for the uranyl-ligand species are given in Table 12. The calculations show that there are positive total binding energies for each of the species. As expected, the tetraanion for $UO_2(CO_3)_3^{4-}$ is less stable than $UO_2(CO_3)_2^{2-}$ in the gas phase due to the excess charge. Clearly, solvation effects must be stabilizing the tricarbonate. What is interesting is that the tricarbonate is a very stable species for the uranyl in solution yet for the Sr^{2+}, the tricarbonate is not predicted to form. This is likely due to the fact that the Sr^{2+} ion is better solvated in the first solvation shell with up to eight waters of solvation as compared to the uranyl for which only up to five waters of solvation are present in the first solvation shell. Thus, it is easier to desolvate the uranyl dication than the Sr^{2+} dication leading to the formation of the tricarbonate in the former and not for the latter. In addition, other counterions may play a role in stabilizing the 4-tricarbonate for the uranyl and may not contribute so much in the case of Sr^{2+}. The total trimer binding energy is 1972.8 kcal/mol relative to six separate CO_3^{2-} species but the trimer with a charge of −6 is less stable than 3 separated $UO_2(CO_3)_2^{2-}$ as isolated species by 461.1 kcal/mol. Again solvation and counterions are expected to play a role in stabilizing the complex in solution.

The complexes with the monanion ligands are all expected to be stable with each cluster being more stable than the preceding one. The acetate complexes get stabilized more than the nitrate complexes on binding to UO_2^{2+} due to less resonance stabilization in the naked acetate anion.

Conclusions

The results clearly indicate that density functional theory with effective core potentials can be used to predict the geometries and vibrational spectra of the complexes of the uranyl dication with a variety of anionic ligands. The local functional DFT (LDFT) approach yields geometrical parameters that are in good agreement with the available EXAFS and X-ray data for the carbonate, nitrate, and acetate species. The calculated vibrational frequencies for the U═O symmetric and asymmetric stretches in the $UO_2(CO_3)_3^{4-}$ anion are in good agreement with experimental data. The calculations suggest that the splitting of the carbonate bands upon complexation with the uranyl cation is really due to the formation of terminal C═O species. The U═O stretching frequencies in the nitrate and acetate monoanionic species are within 20−30 cm^{-1} of experiment for both the symmetric and asymmetric stretches. In the nitrates, the N−O stretches show similar behavior as observed in the carbonates, where complexation with the uranyl cation raises the terminal N−O stretching frequency by more than 300 cm^{-1}, indicative of N═O formation. The acetates also show interesting behavior, with the highest C−O modes increasing with the addition of more acetates around the uranyl cation.

Acknowledgment. This research was performed in part using the Molecular Science Computing Facility (MSCF) in the William R. Wiley Environmental Molecular Sciences Laboratory, a national scientific user facility sponsored by the U. S. Department of Energy's Office of Biological and Environmental Research and located at the Pacific Northwest National Laboratory, operated for the Department of Energy by Battelle. This research was supported in part by the U. S. Department of Energy's the Mathematical, Information, and Computational Science Division phase II grand challenges of the Office of Computational and Technology Research and in part by the Environmental Management Sciences Program (EMSP) of the Department of Energy under a project entitled "Chemical Speciation of Strontium, Americium, and Curium in High Level Waste", Project No. 26753. David A. Dixon is indebted to the Robert Ramsay Endowment of the University of Alabama.

Supporting Information Available: The atomic coordinates for the optimized geometries and the complete set of vibrational frequencies (and their assignments) are available. This material is available free of charge via the Internet at http://pubs.acs.org.

References and Notes

(1) Allen, P. G.; Bucher, J. J.; Clark, D. L.; Edelstein, N. M.; Ekberg, S. A.; Gohdes, J. W.; Hudson, E. A.; Kaltsoyannis, N.; Lukens, W. W.; Neu, M. P.; Palmer, P. D.; Reich, T.; Shuh, D. K.; Tait, C. D.; Zwick, B. D. *Inorg. Chem.* **1995**, *34*, 4797.

(2) Docrat, T. I.; Mosselmans, J. F. W.; Charnock, J. M.; Whiteley, M. W.; Collison, D.; Livens, F. R.; Jones, C.; Edmiston, M. J. *Inorg. Chem.* **1999**, *38*, 1879.

(3) Amayri, S.; Arnold, T.; Reich, T.; Foerstendorf, H.; Geipel, G.; Bernard, G.; Massanek, A. *Environ. Sci. Technol.* **2004**, *38*, 6032.

(4) Amayria, S.; Reicha, T.; Arnoldb, T.; Geipelb, G.; Bernhard, G. *J. Solid State Chem.* **2005**, *178*, 567.

(5) Frost, R. L.; Erickson, K. L.; Weier, M. L.; Carmody, O.; Cejka, J. *J. Mol. Struct.* **2005**, *737*, 173.

(6) Taylor, J. C.; Mueller, M. H. *Acta Crystallogr.* **1965**, *19*, 536.

(7) Brooker, M. H.; Huang, C.-H.; Sylwestrowicz, J. *J. Inorg. Nucl. Chem.* **1980**, *42*, 1431.

(8) Nguyen-Trung, C.; Begun, G. M.; Palmer, D. A. *Inorg. Chem.* **1992**, *31*, 5280.

(9) De Houwer, S.; Gorller-Walrand, C. *J. Alloys Compd.* **2001**, *683*, 323.

(10) Pyykkö, P.; Li, J.; Runeberg, N. *J. Phys. Chem.* **1994**, *98*, 4809.

(11) Gagliardi, L.; Grenthe, I.; Roos, B. I. *Inorg. Chem.* **2001**, *40*, 2976.

(12) Vázquez, J.; Bo, C.; Poblet, J. M.; de Pablo, J.; Bruno, J. *Inorg. Chem.* **2003**, *42*, 6136.

(13) Tsushima, S.; Uchida, Y.; Reich, T. *Chem. Phys. Lett.* **2002**, *357*, 73.

(14) Majumdar, D.; Balasubramanian, K.; Nitsche, H. *Chem. Phys. Lett.* **2002**, *361*, 143.
(15) Majumdar, D.; Roszak, S.; Balasubramanian, K.; Nitsche, H. *Chem. Phys. Lett.* **2003**, *372*, 232.
(16) Hemmingsen, L.; Amara, P.; Ansoborlo, E.; Field, M. J. *J. Phys. Chem. A* **2000**, *104*, 4095.
(17) Ryzhkov, M. V.; Gubanov, V. A. *J. Radioanal. Nucl. Chem.* **1990**, *143*, 85.
(18) Craw, J. S.; Vincent, M. A.; Hillier, I. H.; Wallwork, A. L. *J. Phys. Chem.* **1995**, *99*, 10181.
(19) Hirata, M.; Monjyushiro, H.; Sekine, R.; Onoe, J.; Nakamatsu, H.; Mukoyama, T.; Adachi, H.; Takeuchi, K. *J. Electron Spectrosc. Related Phenom.* **1997**, *83*, 59.
(20) Hirata, M.; Tachimori, S., Sekine R., Onoe J.; Nakamatsu, H. *Adv. Quantum Chem.* **2001**, *37*, 335.
(21) Oda, Y.; Funasaka, H.; Nakamura, Y.; Adachi, H. *J. Alloys Compd.* **1997**, *255*, 24.
(22) Nitsche, H.; Silva, R. J.; Brendler, V.; Geipel, G.; Reich, T.; Teterin, Y. A.; Thieme, M.; Baraniak, L.; Bernhard, G. "Actinide Speciation" in *High Ionic Strength Media. Experimental and modeling approaches to predict actinide speciation and migration in the subsurface*; Reed, D. T., Clark, S. B., Rao, L., Eds.; Kluwer Academic/PlenumPublishers: New York, 1999.
(23) Bailey, E. H.; Mosselmans, J. F. W.; Schofield P. F. *Geochim. Cosmochim. Acta* **2004**, *68*, 1711.
(24) Denecke, M. A.; Reich, T.; Bubner, M.; Pompe, S.; Heise, K. H.; Nitsche, H.; Allen, P. G.; Bucher, J. J.; Edelstein, N. M.; Shuh, D. K. *J. Alloys Compd.* **1998**, *271*−*273*, 123−127.
(25) Jiang, J.; Rao, L.; Di Bernardo, P.; Zanonato, P. L.; Bismondo, A. *J. Chem. Soc., Dalton Trans.* **2002**, 1832.
(26) Templeton, D. H.; Zalkin, A.; Ruben, H.; Templeton, L. K. *Acta Crystallogr.* **1985**, *C41*, 1439.
(27) Navaza, A.; Charpin, P.; Vigner, D.; Heger, G. *Acta Crystallogr. C* **1991**, *47*, 1842.
(28) Silva, M. R.; Beja, A. M.; Paixão, J. A.; Da Veiga, L. A.; Martin-Gil, J. *Acta Crystallogr. C* **1999**, *55*, 2039.
(29) Zalkin, A.; Ruben, H.; Templeton, D. H. *Acta Crystallogr. B* **1982**, *38*, 610.
(30) Quilès, F.; Burneau, A. *Vib. Spec.* **1998**, *18*, 61.
(31) (a) Parr, R. G.; Yang, W. *Density Functional Theory of Atoms and Molecules*, Oxford University Press: New York, 1989; (b) Labanowski, J., Andzelm, J., Eds. *Density Functional Methods in Chemistry*; Springer-Verlag: New York, 1991.
(32) Sosa, C.; Andzelm, J.; Elkin, B. C.; Wimmer, E.; Dobbs, K. D.; Dixon, D. A. *J. Phys. Chem.*, **1992**, *96*, 6630; Christe, K. O.; Dixon, D. A.; Mack, H. G.; Oberhammer, H.; Pagelot, A.; Sanders, J. C. P.; and Schrobilgen, G. J. *J. Am. Chem. Soc.* **1993**, *115*, 11279; Casteel, W. J., Jr.; Dixon, D. A.; LeBlond, Mercier, H. P. A.; Schrobilgen, G. J. *Inorg. Chem.* **1998,** *37*, 340; Rustad, J. R.; Dixon, D. A.; Russo, K.; Felmy, A. R. *J. Am. Chem. Soc.* **1999**, *121*, 3234.
(33) Ziegler, T. *Chem. Rev.* **1991**, *91*, 651.
(34) Salahub, D. R. In *Ab Initio Methods in Quantum Chemistry* −*II*; Lawley, K. P., Ed.; John Wiley & Sons: New York, 1987, p 447.
(35) Schreckenbach, G.; Hay, P. J.; Martin, R. L. *J. Comput. Chem.* **1999**, *20*, 70; Hay, P. J.; Martin, R. L. *J. Chem. Phys.* **1998**, *109*, 3875.
(36) Slater, J. C. *Phys. Rev.* **1951**, *81*, 385.
(37) Vosko, S. H.; Wilk, L.; Nusair, M. *Can. J. Chem.* **1980**, *58*, 1200.
(38) Becke, A. D. *J. Chem. Phys.* **1993**, *98*, 5648.
(39) Lee, C.; Yang, W.; Parr, R. G. *Phys. Rev. B* **1988**, *37*, 785.
(40) de Jong, W. A.; Harrison, R. J.; Nichols, J. A.; Dixon, D. A. *Theor. Chem. Acc.* **2001**, *107*, 22.
(41) Fuentealba, P.; Preuss, H.; Stoll, H.; Szentpaly, L. V. *Chem. Phys. Lett.* **1982**, *89*, 418; Fuentealba, P.; Szentpaly, L. V.; Preuss, H.; Stoll, H. *J. Phys. B* **1985**, *18*, 1287; Igel-Mann, G., Stoll, H.; Preuss, H. *Mol. Phys.* **1988**, *65*, 1321; Kuechle, W.; Dolg, M.; Stoll, H.; Preuss, H. *Mol. Phys.* **1991**, *74*, 1245; Kaupp, M.; Schleyer, P. V. R.; Stoll, H.; Preuss, H. *J. Chem. Phys.* **1991**, *94*, 1360; Bergner, A.; Dolg, M.; Kuechle, W.; Stoll, H.; Preuss, H. *Mol. Phys.* **1993**, *80*, 1431; Dolg, M.; Stoll, H.; Preuss, H.; Pitzer, R. M. *J. Phys. Chem.* **1993**, *97*, 5852; Küchle, W.; Dolg, M.; Stoll, H.; Preuss, H. *J. Chem. Phys.* **1994**, *100*, 7535.
(42) Godbout, N.; Salahub, D. R.; Andzelm, J.; Wimmer, E. *Can. J. Chem.* **1992**, *70*, 560.
(43) Perdew, J. P.; Burke, K.; Ernzerhof, M. *Phys. Rev. Lett.* **1996**, *77*, 3865; Perdew, J. P.; Burke, K.; Ernzerhof, M. *Phys. Rev. Lett.* **1997**, *78*, 1396.
(44) Dunlap, B. I.; Connolly, J. W. D.; Sabin, J. R. *J. Chem. Phys.* **1979**, *71*, 4993.
(45) Aprà, E.; Windus, T. L.; Straatsma, T. P.; Bylaska, E. J.; de Jong, W.; Hirata, S.; Valiev, M.; Hackler, M.; Pollack, L.; Kowalski, K.; Harrison, R.; Dupuis, M.; Smith, D. M. A.; Nieplocha, J.; Tipparaju V.; Krishnan, M.; Auer, A. A.; Brown, E.; Cisneros, G.; Fann, G.; Fruchtl, H.; Garza, J.; Hirao, K.; Kendall, R.; Nichols, J.; Tsemekhman, K.; Wolinski, K.; Anchell, J.; Bernholdt, D.; Borowski, P.; Clark, T.; Clerc, D.; Dachsel, H.; Deegan, M.; Dyall, K.; Elwood, D.; Glendening, E.; Gutowski, M.; Hess, A.; Jaffe, J.; Johnson, B.; Ju, J.; Kobayashi, R.; Kutteh, R.; Lin, Z.; Littlefield, R.; Long, X.; Meng, B.; Nakajima, T.; Niu, S.; Rosing, M.; Sandrone, G.; Stave, M.; Taylor, H.; Thomas, G.; van Lenthe, J.; Wong, A.; Zhang, Z.; "NWChem, A Computational Chemistry Package for Parallel Computers, Version 4.7" 2005, Pacific Northwest National Laboratory, Richland, WA 99352-0999, USA.; Kendall, R. A.; Apra, E.; Bernholdt, D. E.; Bylaska, E. J.; Dupuis, M.; Fann, G. I.; Harrison, R. J.; Ju, J.; Nichols, J. A.; Nieplocha, J.; Straatsma, T. P.; Windus, T. L.; Wong, A. T. *Computer Phys. Comm.* **2000**, *128*, 260−283.
(46) Gaussian 03, Revision B.05, Frisch, M. J.; Trucks, G. W.; Schlegel, H. B.; Scuseria, G. E.; Robb, M. A.; Cheeseman, J. R.; Montgomery, J. A., Jr.; Vreven, T.; Kudin, K. N.; Burant, J. C.; Millam, J. M.; Iyengar, S. S.; Tomasi, J.; Barone, V.; Mennucci, B.; Cossi, M.; Scalmani, G.; Rega, N.; Petersson, G. A.; Nakatsuji, H.; Hada, M.; Ehara, M.; Toyota, K.; Fukuda, R.; Hasegawa, J.; Ishida, M.; Nakajima, T.; Honda, Y.; Kitao, O.; Nakai, H.; Klene, M.; Li, X.; Knox, J. E.; Hratchian, H. P.; Cross, J. B.; Bakken, V.; Adamo, C.; Jaramillo, J.; Gomperts, R.; Stratmann, R. E.; Yazyev, O.; Austin, A. J.; Cammi, R.; Pomelli, C.; Ochterski, J. W.; Ayala, P. Y.; Morokuma, K.; Voth, G. A.; Salvador, P.; Dannenberg, J. J.; Zakrzewski, V. G.; Dapprich, S.; Daniels, A. D.; Strain, M. C.; Farkas, O.; Malick, D. K.; Rabuck, A. D.; Raghavachari, K.; Foresman, J. B.; Ortiz, J. V.; Cui, Q.; Baboul, A. G.; Clifford, S.; Cioslowski, J.; Stefanov, B. B.; Liu, G.; Liashenko, A.; Piskorz, P.; Komaromi, I.; Martin, R. L.; Fox, D. J.; Keith, T.; Al-Laham, M. A.; Peng, C. Y.; Nanayakkara, A.; Challacombe, M.; Gill, P. M. W.; Johnson, B.; Chen, W.; Wong, M. W.; Gonzalez, C.; Pople, J. A.; Gaussian, Inc., Wallingford CT, 2004.
(47) Reed, A. E.; Curtiss, L. A.; Weinhold, F. *Chem. Rev.* **1988**, *88*, 899; Foster, J. P.; Weinhold, F. *J. Am. Chem. Soc.* **1980**, *102*, 7211; Reed, A. E.; Weinhold, F. *J. Chem. Phys.* **1983**, *78*, 4066; Reed, A. E.; Weinstock, R. B.; Weinhold, F. *J. Chem. Phys.* **1985**, *83*, 735; Reed, A. E.; Weinhold, F. *J. Chem. Phys.* **1985**, *83*, 1736.
(48) Mereiter, K. *Acta Crystallogr.* **1998**, *C44*, 1175.
(49) Coda, A.; Della Giusta, A.; Tazzoli, V. *Acta Crystallogr.* **1981**, *B37*, 1496.
(50) Meinrath, G. *J. Radioanal. Nucl. Chem.* **1996**, *211(2)*, 349.
(51) Anderson, A.; Chieh, C.; Irish, D. E.; Tong, J. P. K. *Can. J. Chem.* **1980**, *58*, 1651.
(52) Reeder, R. J.; Nugent, M.; Lamble, G. M.; Tait, C. D.; Morris, D. E. *Environ. Sci. Technol.* **2000**, *34(4)*, 638.
(53) Aberg, M.; Ferri, D.; Glaser, J.; Grenthe, I. *Inorg. Chem.* **1983**, *22*, 3981.
(54) Cromer, D. T.; Harper, P. E. *Acta Crystallogr.* **1955**, *8*, 847.
(55) Basile, L. J.; Ferraro, J. R.; Mitchell, M. L.; Sullivan, J. C. *Appl. Spectrosc.* **1978**, *32*, 535.
(56) Madic, C.; Hobart, D. E.; Begun, G. M. *Inorg. Chem.* **1983**, *22*, 1494.
(57) Anderson, A.; Chieh, C.; Irish, D. E.; Tong, J. P. K. *Can. J. Chem.* **1980**, *58*, 1651.
(58) Koglin, E.; Schenk, H. J.; Schwochau, K. *Spectrochim. Acta*, **1979**, *35A*, 641.
(59) Barclay, G. A.; Sabine, T. M.; Taylor, J. C. *Acta Crystallogr.* **1965**, *19*, 205.
(60) Zivadinovic, M. S. *Bull. Boris Kidric Inst. Nucl. Sci.* **1967**, *18*, 1.
(61) Krivovichev, S. V.; Burns, P. C. *Radiochemistry* **2004**, *46*, 16.
(62) Hughes, K.-A.; Burns, P. C. *Acta Crystallogr., Sect. C* **2003**, *59*, i7.
(63) McGlynn, S. P.; Smith, J. K.; Neely, W. C. *J. Chem. Phys.* **1961**, *35(1)*, 105.
(64) Brooker, M. H.; Huang, C.-H.; Sylwestrowicz, J. *J. Inorg. Nucl. Chem.* **1980**, *42*, 1431.
(65) Jones, L. H. *Spectrochim. Acta* **1959**, *14*, 409; Jones, L. H. *J. Chem. Phys.* **1955**, *23*, 2105.
(66) Gál, M.; Goggin, P. L.; Mink, J. *Spectrochim Acta* **1992**, *48A*, 121.
(67) Kline, R. J.; Kershner, C. J. *Inorg. Chem.* **1966**, *5*, 932.
(68) Felmy, A. R.; Dixon, D. A.; Rustad, J. R.; Mason, M. J.; Onishi, L. M. *J. Chem. Thermo.* **1998**, *30*, 1103.